Numerical validation of a new method to assess aortic pulse wave velocity from a single recording of a brachial artery waveform with an occluding cuff.

B. Trachet[1], P. Reymond[2], J. Kips[1,3], A. Swillens[1], M. De Buyzere[4], B. Suys[5], N. Stergiopulos[2], P. Segers[1].

[1] Ghent University, bioMMeda - IBiTech, Ghent, Belgium

[2] Swiss Federal Institute of Technology, Laboratory of Hemodynamics and Cardiovascular Technology, Lausanne, Switzerland

[3] Ghent University Hospital, Department of Pharmacology, Ghent, Belgium

[4] Ghent University Hospital, Department of Cardiovascular Diseases, Ghent, Belgium

[5] Antwerp University, Department of Pediatrics, Antwerp, Belgium

Running Head: Numerical validation of a new method to assess PWV

Bram Trachet

bioMMeda - Institute Biomedical Technology – Ghent University

De Pintelaan 185, Block B

BE-9000 Gent (Belgium)

Tel: +32 9 332 33 79

Fax: +32 9 332 41 59

bram.trachet@ugent.be

Abstract

Recently a new method has been proposed as a tool to measure arterial pulse wave velocity (PWV), a measure of the stiffness of the large arteries and an emerging parameter used as indicator of clinical cardiovascular risk. The method is based on measurement of brachial blood pressure during supra-systolic pressure inflation of a simple brachial cuff (the device is known as the Arteriograph (Tensiomed, Budapest, Hungary)). This occlusion yields pronounced first and secondary peaks in the pressure waveform, the latter ascribed to a reflection from the aortic bifurcation, and PWV is calculated as the ratio of twice the jugulum-symphysis distance and the time difference between the two peaks. To test the validity of this working principle we used a numerical model of the arterial tree to simulate pressures and flows in the normal configuration, and in a configuration with an occluded brachial artery**.** A pronounced secondary peak was indeed found in the brachial pressure signal of the occluded model, but its timing was only related to brachial stiffness and not to aortic stiffness. We also compared PWV's calculated with 3 different methods: PWV_{ATG} (~ Arteriograph principle), $PWV_{car\text{-}fem}$ (~ carotid-femoral PWV, the current clinical gold standard method) and PWV_{theor} (~ Bramwell-Hill equation). Both PWV_{ATG} (R^2=0.94) and $PWV_{car\text{-}fem}$ (R^2=0.95) correlated well with PWV_{theor}, but their numerical values were lower (by 2.17 ± 0.42 and 1.08 ± 0.70 m/s for PWV_{ATG} and $PWV_{car\text{-}fem}$, respectively). In conclusion, our simulations question the working principle of the Arteriograph. Our data indicate that the method picks up wave reflection phenomena confined to the brachial artery, and derived values of PWV rather reflect the stiffness of the brachial arteries.

Keywords— Wave reflections, arterial network model, heart model, wave propagation, wave intensity analysis, pressure waveforms, pulse wave velocity, arterial stiffness.

Introduction

With the increased attention for large artery stiffness and the obvious role of arterial stiffening in the patho-physiology of (isolated) systolic hypertension, the 2007 ESC and ESH guidelines for the management of arterial hypertension [4] now formally recognize large artery stiffness as a factor influencing the prognosis of patients, and measurement of arterial stiffness as a useful indicator of vascular damage. Large consensus exists that of all available methods to quantify arterial stiffness or aspects of it, measurement of (carotid-femoral) pulse wave velocity (PWV) is, at present, the only non-invasive comprehensive method which is simple and accurate enough to be considered as a diagnostic procedure feasible on a large scale in a clinical setting, with high values being indicative of stiffened arteries [4,9]. In essence, measurement of PWV is simple and straightforward, and it is calculated as the ratio of the distance between two measuring locations and the time it takes for the waves to travel from one location to the other (the pulse transit time). And yet, there is still much ambiguity in measuring PWV, arising on the one hand from difficulties in accurate measurement of the transit time and identification of the foot of the wave front, and on the other hand from measuring the actual travel distance of the waves. The latter is particularly ambiguous for carotid-femoral PWV, where at the moment the wave is picked up at the carotid artery, it is already travelling further down the aorta towards the femoral artery.

With the Arteriograph (Tensiomed, Budapest, Hungary), a new method (and device) to measure pulse wave velocity has recently been introduced onto the market. Unlike most other devices aiming to measure PWV, this device measures the pulse waves at one single location. The device makes use of a brachial cuff that is over-inflated to 35 mmHg over the systolic blood pressure. It is claimed that, as a result of this over-inflation, the reflected wave from the

lower body can be detected more easily. The time difference between the first systolic wave and the second reflected wave is then used as the transit time, i.e., the time needed for the wave to travel back and forth to the reflection site. Assuming that the measured external distance from jugulum to symphysis can be used as an approximation of the distance to this reflection site, pulse wave velocity can be computed as the ratio of travelled distance over transit time.

Validation data on the Arteriograph are still rather limited, but they seem to suggest that there is a relation between PWV measured by this new device and PWV measured by more generally accepted methods. However, the underlying principle of this intriguing method is still not fully understood, since no clear explanation has been given for the appearance of a pronounced second peak when the brachial cuff is over-inflated. This second peak is assumed to originate from a reflection of the pressure wave in the lower body, but no reasonable explanation for the fact that this reflection is more pronounced in the case of an over-inflated brachial artery cuff has yet been published. Furthermore, little is known about the underlying assumptions one has to make to calculate PWV with the Arteriograph.

The principal aim of this work is to gain a better understanding and validation of the working principle behind this new method. We used a computer model of the arterial tree to simulate pressure and flow waveforms in a normal arterial system, and in a configuration representing an over-inflated brachial artery (occluded model). The pressure waveforms and wave reflection patterns in the occluded model were studied, and transit time and PWV calculated using the Arteriograph method were compared to the actual transit time and PWV for different stiffness values in the model.

Materials and methods

Arteriograph: principle of operation

The Arteriograph is basically a simple upper arm cuff connected to a piezoelectric sensor that picks up the pressure signals. Upon operation, the cuff is inflated to a pressure 35 mmHg over the systolic blood pressure. The pressure in the underlying occluded artery is transmitted through the cuff to the pressure sensor and is reported to show multiple peaks (see Figure 1). The first is the systolic peak, corresponding to the ejection of blood from the left ventricle into the aorta, while the second peak is assumed to originate from a reflection of the first pressure wave in the lower body. The time difference between the first and second wave in the pressure signal is used as the return time $\Delta T_{s1\text{-}s2}$, i.e. the time needed for the pressure wave to travel from the aortic arch to its reflection point and back, with the iliac bifurcation assumed to be the dominant reflection point. The exact algorithm used by the device to determine the transit time is unknown but for our analysis we systematically used the peak-to-peak time difference. The travelled distance corresponding to this return time is twice the distance from aortic arch to iliac bifurcation, which is approximated by measuring the distance between jugulum and symphysis externally (see Figure 1).

Computer model simulations of Arteriograph measurements

Model simulations

To gain a better insight into the origin of the pressure waveforms occurring during the over-inflation phase of the Arteriograph, we simulated pressure and flow waveforms in the arterial tree using an improved version [15] of the original 1D model of Stergiopulos *et al* [19]. This model is based on the one-dimensional flow equations and includes nonlinearities arising from

geometry and material properties. One hundred and three (103) arterial segments, representing the various major arteries, are combined and terminated with 3-element windkessel models to form a model of the arterial system. For each segment, properties such as compliance, diameter and length can be adjusted. Resistance can be altered in the distal windkessel models. We refer to Reymond *et al* [15] for details on the properties of individual segments and the computational methods used to solve the 1-D Navier-Stokes equations. We used this model to simulate pressure and flow in the normal configuration, and in a configuration with the left brachial artery completely occluded (~over-inflation of the Arteriograph cuff). The superfluous segments of the brachial artery were thus removed, resulting in an adjusted model containing only 99 segments (see Figure 2).

The pulse wave velocity in the model was assessed in three different ways. First, PWV was determined by measuring the foot-to-foot transit time between the pressure signals at the carotid and femoral arteries ($PWV_{car\text{-}fem}$). The foot of the pressure waveform was determined as the maximum of its second derivative [6,12]. The distance between two nodes could be determined by adding up the lengths of the different segments that connect these nodes. The carotid-femoral distance was then determined as the distance from the aortic root to the femoral artery minus the distance from aortic root to carotid artery, thus correcting for the time the waves are travelling in the opposite direction. The resulting distance was 52.8 cm. Second, the theoretical PWV value for each segment was calculated from the model parameters as $PWV = \frac{1}{\sqrt{\rho \cdot D}}$, with ρ the blood density (1050 kg/m³ in the model) and D the distensibility of the segment. A description of how segment distensibility was determined has been provided by Reymond *et al* [15]. Averaging of PWV for all segments of the aorta, weighted according to the segment lengths, yielded the theoretical PWV which we considered as the gold standard in this work (PWV_{theor}). In a third approach, PWV was calculated using the Arteriograph method: the distance from jugulum to symphysis was approximated by

adding the segment lengths from the thoracic aorta (starting just after the branch towards the occluded brachial artery) to the aorto-iliac bifurcation, resulting in 37.5 cm. Twice this distance was divided by the transit time between the two peaks in the pressure signal (see also Figure 1) to find values for pulse wave velocity, PWV_{ATG}.

All simulations were performed for 6 different levels of stiffness of the model, obtained via multiplication of the default compliance value of each segment with a constant compliance factor, changing the compliance from 40% to 140% of its default value in steps of 20%. By changing the compliance in each segment of the arterial tree, we were able to assess the influence of the arterial stiffness on the pulse wave velocity in both configurations of the model. Apart from the compliance of the segments, three more model parameters were varied to test the robustness of the methodology. Extra simulations were run on the occluded model by changing the default arterial resistance of each terminal windkessel to 80% and 120% of its original value, by changing the duration of a heart cycle to 0.7 and 0.9 seconds instead of the original 0.8 seconds and by changing the maximal elastance (E_{max}) of the heart model to 1.5 and 3.5 mmHg/ml instead of the default value of 2.5 mmHg/ml. This allowed us to compute 7 different PWV-values for each compliance level. We thus found a cloud of PWV's for each of the three methods, and these were analysed using Bland-Altman analysis.

To further test the method's sensitivity to isolated changes in stiffness along the brachial trajectory, 2 extra simulations were performed: in a first simulation only the compliance of the brachial segments was changed (from 40% to 140% of its default value in steps of 20%) while all other segments maintained their default compliance value. In a second simulation compliance was changed for all segments in the arterial tree except the brachial ones.

For both the occluded and the original model, pressure and flow waveforms were calculated at 5 equidistant locations along the brachial artery using the default model parameters (default

compliance and resistance values, heart cycle of 0.8 s, E_{max} of 2.5 mmHg/ml). Furthermore, we also calculated similar data at 5 locations along the ascending, descending and abdominal aorta to investigate whether the propagation of the reflected waves in the abdominal aorta was similar in both models. The obtained pressure and flow waveforms were further processed in Matlab (Mathworks, Natick, MA) [16,18] .

Data and wave reflection analysis

We performed wave intensity analysis on the pressure and flow signals of a simulation on the occluded model with default parameters (default compliance and resistance values, heart cycle of 0.8 s, E_{max} of 2.5 mmHg/ml) to gain more insight into the nature and origin of the different peaks occurring in the signals [14,20]. The theory of wave intensity analysis was elaborated by Parker and Jones [14] and we refer to their work for details on the method. In brief, disturbances to the flow lead to changes in pressure (dP) and flow velocity (dU), ‘‘wavelets’’, which propagate along the vessels with a wave speed (PWV). Each wavelet is, in its turn, composed of a forward (subscript +) and backward (subscript -) running component, related by $dP\pm = PWV \cdot \rho \cdot dU \pm$ with PWV the local PWV_{theor} provided by the computer model. Waves characterized by a dP>0, that is a rise in pressure, are called compression waves, while waves with dP <0 are expansion or suction waves. The nature of a wave was further assessed by analysing the wave intensity, dI, which is defined as the product of dU and dP, and equals the rate of energy flux carried by the wavelet. When dI is positive forward waves are dominant; negative dI indicates dominant backward waves. Wave intensity in itself was then also separated in a net forward and backward wave intensity: $dI_+ = dP_+ \cdot dU_+$ and $dI_- = dP_- \cdot dU_-$, where the ‘‘+’’ denotes a forward travelling wave, while ‘‘-’’ denotes a backward travelling wave. After having computed forward and backward intensity waves in

the brachial artery, we computed the distance travelled by these waves to their reflection point. In order to do so, the transit time ΔT between a forward wave and its backward reflection is combined with the local theoretical PWV in the brachial artery. Since the wave is travelling back and forth to its reflection site, this allows us to compute the distance to the reflection site as $L = \frac{\Delta T \cdot PWV_{theor}}{2}$.

Beside the wave intensity analysis, we also determined the forward and backward pressure components at different locations in the aortic trunk and in the brachial artery to unravel the patterns of wave reflection in the normal and occluded configuration. Pressure (P) and flow (Q) can be considered to be composed of one forward running component P_f (Q_f) and one backward running component P_b (Q_b), where the single forward and backward running components are the resultant of all forward and backward travelling waves. These forward and backward components were derived as [23]:

$$P_f = \sum dP +$$
$$P_b = \sum dP -$$

Results

Computer model simulations

Effect of brachial artery occlusion on the pressure waveform

Figure 3 shows pressure waveforms at the distal end of the brachial artery (immediately proximal to the occlusion site) for both the control (top left) and the occluded model (top right). To assess the influence of the stiffness of the arteries on the obtained pulse wave velocity the pressure signals were computed for 6 different levels of arterial compliance, keeping all other model parameters on their default value. The time delay between the first and second systolic peak in the occluded model $\Delta T_{s1\text{-}s2}$, that should be related to aortic PWV according to the Arteriograph principle (see Figure 1), decreased from 0.271 s to 0.123 s for compliance decreasing from 140% to 40% of its original value (not all values shown in Figure 3 to improve visibility).

Figure 3 also shows the resulting brachial pressure waveforms when compliance of the occluded model is only altered in the brachial segments (bottom left), and in all segments except the brachial ones (bottom right). It is observed that $\Delta T_{s1\text{-}s2}$ is proportional to the change in compliance when compliance was altered in all segments and when it was altered in the brachial segments only, but there was no change in the time delay between the first and second systolic peaks when the compliance in the brachial segments was not altered.

Impact of model stiffness, resistance and cardiac parameters on PWV

In Figure 4, the three methods used to determine PWV are compared. For all methods, PWV increased significantly over the simulated range, varying from about 5.2 m/s to 9.2 m/s (theoretically calculated values). This is consistent with a nearly 4-fold decrease in total arterial compliance. There was a good correlation between PWV_{theor} and $PWV_{car\text{-}fem}$ (R^2=0.95), but $PWV_{car\text{-}fem}$ was systematically lower than PWV_{theor} (difference: 1.08 ± 0.70 m/s). Bland-Altman analysis showed that the underestimation increased with higher values of PWV (Figure 4).

There was also a good correlation between the theoretical pulse wave velocities and those calculated using the Arteriograph method (R^2=0.94), but again PWV_{ATG} was lower than PWV_{theor} (difference: 2.17 ± 0.42 m/s), the underestimation increasing with higher values of PWV (Figure 4). Comparing $PWV_{car\text{-}fem}$ with PWV_{ATG}, both methods correlate well (R^2=0.90), with $PWV_{car\text{-}fem}$ being on average 1.09 ± 0.48 m/s higher than PWV_{ATG}. The difference between both, however, becomes smaller with higher values of PWV. We conclude that, although PWV_{ATG} correlates well with both PWV_{theor} and $PWV_{car\text{-}fem}$, the numerical values of the Arteriograph method are clearly lower than those of the other methods.

Reducing the resistance of each terminal windkessel to 80 % of its default value resulted in a decrease of mean blood pressure and, given the non-linear coupling between blood pressure and stiffness, a lowering in PWV with 8 ± 3 % of its initial value (average normalized difference ± SD for 18 simulated cases: 3 different methods and 6 compliance levels per method). Increasing the resistance to 120 % of its initial value increased PWV with 7 ± 4 %. Shortening the heart cycle from 0.8 s to 0.7 s resulted in an increase in (blood pressure and) PWV with 5 ± 3 % of its initial value, whereas PWV decreased with 6 ± 3 % when the heart cycle was elongated to 0.9 s. Finally, PWV values decreased with 14 ± 7 % when the maximal heart elastance E_{max} was lowered from 2.5 mmHg/ml to 1.5 mmHg/ml, and PWV

values increased with 9 ± 5 % when Emax was raised to 3.5 mmHg/ml. These changes were again modulated by the changes in operating blood pressure.

What is causing the change in transit time?

In Figure 5 the influence on PWV_{ATG} of altering compliance in only the brachial segments is compared to the influence of altering compliance in all but the brachial segments. When compliance is decreased in all but the brachial segments, PWV_{theor} and $PWV_{car\text{-}fem}$ increase but PWV_{ATG} remains constant. This can also be observed in Figure 3 (bottom right), since transit times did not change in the occluded model when compliance in the brachial segment was kept at its original value. Similar results are found by altering compliance only in the segments of the aortic trunk, where most of the compliance of the arterial system resides (not plotted). On the other hand, increasing compliance only in the brachial artery results in an increase of PWV_{ATG} whereas PWV_{theor} and $PWV_{car\text{-}fem}$ obviously remain constant since stiffness in the aorta is not changing. We also observe that the corresponding transit times (and resulting PWV_{ATG} values) are identical to the simulation where compliance in all segments was altered. This implies that all correlations between PWV_{ATG} and PWV_{theor} or $PWV_{car\text{-}fem}$ as they are plotted in Figure 4 are modulated by the local change in stiffness in the (occluded) brachial artery and not by the change in aortic stiffness of the complete model as such.

To further investigate the origin of the second peak in the pressure signal of the occluded model, the pressure waveforms and their forward and backward components are compared on 5 different locations throughout the brachial artery (Figure 6) and the aortic trunk (Figure 7). This was done for both the normal and the occluded model using default parameters. In Figure 6, the timing of the forward waveforms throughout the brachial artery is similar in both models: the more distal in the brachial artery, the greater the time delay since the pressure

wave arrives later. The amplitude of the forward waveforms is similar in both models, depending on the compliance. In the backward waveforms, more important differences between both configurations can be noticed. The amplitude of the backward components in the occluded model is much higher. Also in the occluded model, the reflected wave appears first at the occlusion and only later at the proximal part of the brachial artery, while the timing of the backward component is scattered in the non-occluded configuration.
Studying the waveforms (and the forward and backward components) along the aortic trunk (Figure 7) did not reveal obvious differences between the occluded and non-occluded configuration. This is another indication that the second peak in the pressure signal is probably caused by a local phenomenon in the brachial artery, and is not linked to waves travelling back from the lower body.

Wave intensity analysis

The results of the wave intensity analysis performed on the pressure and flow signals just proximal to the occlusion of the brachial artery are shown in Figure 8. Analysis of the normal model reveals a forward compression wave (P_1), arising from the systolic ejection. This wave is followed by a backward compression wave (P_2), a (positive closed end) reflection of the first forward wave in the brachial artery itself. Then there is a forward expansion wave (P_3) linked with the relaxation of the left ventricle. Performing the same analysis for the model of an occluded brachial artery reveals that now the peak intensity of the first backward compression wave (P'_2) is almost three times stronger than in the original model. This strong backward compression wave is caused by the total reflection of the incident wave on the brachial occlusion. Next, we observe a forward expansion wave P_3', that is most probably a reflection of P_2'. To assess the origin of this reflection, the distance travelled by the reflected

wave was calculated. Combining the peak-to-peak time difference between P_3' and P_2' and the local theoretical PWV in the brachial segment, the distance from the measurement point to the reflection point was determined to be 29.5 cm. This distance approximates the distance to the point where the subclavian artery, later becoming the brachial artery, branches from the aortic arch (35.05 cm upstream from the location where wave intensity analysis is performed). We therefore hypothesize that the reflected backward compression wave P_2' is re-reflected at the location where the subclavian branches from the aorta, and is picked up at the location of the cuff as the forward expansion wave P_3'. Next, P_4' is a backward expansion wave caused by the reflection of P_3' on the occlusion and P_5' is again a forward compression wave, caused by the reflection of P_4'. The distance matching the peak-to-peak transit time between P_4' and P_5' is 30.2 cm, thus we can reasonably assume that this wave is reflected at the same point as the previous wave. It is obvious from the timing in Figure 8 that P_5' is the wave causing the pronounced second peak in the pressure signal picked up by the Arteriograph. Using wave intensity analysis, we have thus shown that P_5' is a forward compression wave, caused by a re-re-re-reflection of the first incident wave. This wave is travelling back and forth between the occlusion of the cuff and the point where the subclavian artery branches from the aortic trunk.

Discussion

The main conclusions that we can draw from this computer model study are: (i) occlusion of the brachial artery introduces a total reflection at the upper arm which introduces a pronounced second peak in the brachial pressure curve; (ii) when compliance of the model is altered over the complete arterial tree, the pulse wave velocity calculated following the Arteriograph principle is lower than but correlates well with both the theoretical and carotid-femoral PWV; (iii) this correlation, however, is modulated by local stiffness modifications in the brachial artery and is not linked to aortic stiffness in the remaining parts of the arterial system.

Our study questions the working principle of the Arteriograph and, at the same time, also raises some concern with respect to the ability of the device to provide accurate values of PWV, comparable to transit-time methods. The main difference between the Arteriograph and most other methods to measure pulse wave velocity from transit times is that the Arteriograph only measures at one location: the upper arm. As such the device has a clear practical advantage over other techniques since it is much easier in use and measurements can be done significantly faster.

As for available in vivo data, in a first validation study, pulse wave velocity measured by the Arteriograph was compared to that of other devices, and a reasonable agreement has been found [1,7,11]. Baulmann *et al* [1] determined PWV on 64 patients with 3 different devices. PWV measured with the Arteriograph was 8.6 ± 1.3 m/s , which was different from that measured by two frequently used transit-time based methods (with measurements on the carotid and femoral artery), i.e., the Complior system ® (10.1 ± 1.7 m/s) but similar to measurements with Sphygmocor® (8.1 ± 1.1 m/s). The differences in PWV were entirely ascribed to different techniques used to determine the travelled distance, since there was no statistical

difference between measured transit times. The correlation between Arteriograph and Complior (p=0.005) and Arteriograph and Sphygmocor (p=0.043) was significantly worse than the correlation between Complior and Sphygmocor (p=0.001). Magometschnig [11] found values of 9.1 ± 1.8 m/s for Arteriograph and 8.4 ± 1.5 m/s for Sphygmocor. However both measurement techniques did not correlate (r=-0.04). . Illyes [8] also measured PWV as a function of age for 2299 patients and found a linear correlation between measured PWV and age (r=0.52). This is in line with the expectations since PWV is known to rise with age.

We tried to match these literature results with the results from the present study. As can be observed from Figure 3, occlusion of the brachial artery introduces a second peak in the brachial pressure curve which, in normal circumstances, is hardly noticeable. This finding supports the basic working principle of the Arteriograph: inflation of the brachial cuff to a supra-systolic pressure occludes the artery and leads to an amplification of the second peak making the signal strong enough to be picked up by the sensor embedded in the cuff.
In Figure 4 the three methods to compute PWV were compared. The excellent correlation between the theoretical PWV and $PWV_{car\text{-}fem}$ indicates that this method, which is often used to measure PWV in vivo since these arteries are relatively easy to access with a tonometer or an ultrasound probe [2,10,13,21], can be sufficiently accurate to determine pulse wave velocities in vivo. Note, however, that the absolute value of PWV provided by this method is also substantially lower than the theoretical PWV. Moreover, the Bland-Altman plot reveals a trend of underestimation of $PWV_{car\text{-}fem}$ for higher values of PWV. We speculate that the discrepancy between the theoretical PWV and $PWV_{car\text{-}fem}$ is due to the fact that the theoretical PWV value, derived from the Bramwell-Hill equation [5], applies to the ideal case of an infinitely long tube ignoring effects of viscous friction and wave reflection. Furthermore, an error is introduced via the ambiguity of the travel path of the carotid and femoral pulse [17].

As for PWV_{ATG} - focusing on the simulations where stiffness is altered to the same degree over the complete arterial territory - the correlation with theoretical PWV is similar (R^2=0.94) but the numerical values are systematically lower than $PWV_{car\text{-}fem}$. The most obvious explanation for this phenomenon is that, despite the fact that the measured transit times correlate well to the actual PWV values, the distance that was used to calculate PWV from these transit-times does not yield correct results. One of the major assumptions made in the Arteriograph is that the second peak in the pressure signal is caused by a reflection of the forward wave at the aorto-iliac bifurcation, which is assumed to be the single reflection point.

In order to further investigate this assumption, we have tried to explain the origin of the secondary peak in the pressure signal of the occluded model by making use of wave intensity analysis (Figure 8). It is particularly the appearance of a third forward wave (P'_5) that is of interest for this analysis. Linking the timing of P'_5 to the pressure signal in Figure 8 shows that this wave is causing the second peak in the pressure signal that is picked up by the Arteriograph and used to determine the PWV_{ATG}. Since both dP and dI are positive, P'_5 is a forward compression wave. At first sight this supports the assumption made in the Arteriograph, since a reflection coming from the lower body should be a compression wave travelling in the forward direction in the brachial artery. However, analyzing the wave intensity results and the distances that correspond with the transit times between the different waves, we see that P'_5 is actually a re-reflection of P'_3, which in turn is a re-reflection of P'_1. Thus, the wave is travelling back and forth between the occlusion and the location where the subclavian artery branches from the aortic arch, and there is no reflection originating from the lower body.

This finding is supported by Figure 5, showing that the correlation between PWV_{ATG} and aortic PWV is entirely due to local stiffness changes in the brachial artery, contradicting the supposed working principle of the Arteriograph. If the second peak in the pressure signal would indeed be caused by a wave travelling back from the lower body, its timing should be influenced by a change in aortic stiffness of the aortic segments it is passing through, which is not the case. Also, this wave should be noticeable in the abdominal aorta waveforms, which is not the case either (Figure 7). In the brachial artery waveforms however, we clearly see a backward travelling wave (Figure 6). All this leads us to conclude that, even though PWV_{ATG} correlates well to PWV_{theor} and $PWV_{car\text{-}fem}$, the underlying principle causing this correlation is probably not a wave reflected from the lower body, but a local reflection occurring in the brachial artery.

The excellent correlation between theoretical PWV and PWV_{ATG} found in Figure 4 is driven by the fact that the stiffness of the brachial arteries and central vessels was changed to the same extent. Also in humans, stiffness of the upper brachial segment is likely to be related to aortic stiffness [3], which might explain some of the reported in vivo findings. On the other hand, especially for the more peripheral, muscular arteries, there might be discrepancies in the evolution of stiffness with age (and disease) compared to the more central, elastic arteries [22]. The key question therefore remains to what extent the arteries in the brachial segment reflect the properties of the large, central aorta. Anyhow, it follows from our analysis that any value of PWV derived from the Arteriograph is, at best, an indirect and unspecific estimate of the stiffness of the aorta.

This is a computer model simulation study with its inherent strengths and limitations.

Its strength lies in the fact that pressure and flow signals can be calculated at every location in the arterial tree with great accuracy without any measurement error. A numerical model, however, remains an approximation of reality: the arterial tree is not modelled into great detail (e.g. the microcirculation has not been taken into account). However the model has been validated and has been shown to produce realistic waveforms [15].Still, the pressure curves that were simulated in this work represent an ideal case and don't take into account any damping of the pressure signals in the cuff nor the damping that will occur in the transmission of the pressure signal from the brachial artery through the skin towards the pressure sensor. Therefore the curves that are actually measured by the Arteriograph will probably show a less distinct second peak, making it harder to recognize and measure the transit time.

In our simulations the left brachial artery was occluded. Typically, the left subclavian artery (later becoming the brachial artery) arises directly from the aortic arch as the third and final of the great vessels, while the right subclavian artery arises from the bifurcation of the brachiocephalic trunk. Therefore occlusion of the right brachial artery might result in slightly different wave reflections, although we don't expect large differences.

The exact algorithm used by the device to determine the transit time and the corresponding pulse wave velocity is unknown. We calculated the transit time from the peak-to-peak time difference between the first and second peak. It is generally agreed upon that the foot-to-foot method usually yields the most accurate results, but it is not always easy to determine the foot of the second peak in the signal. It is unclear what method is used by the Arteriograph to determine the transit time, so it is possible that, provided with the same pressure curves, the device would calculate different transit times.

Conclusions

We have validated the working principle of a newly proposed method to measure aortic pulse wave velocity (the Arteriograph method) using a numerical model of the arterial tree. This method bases its transit time calculation on a second peak in the pressure signal of the over-inflated brachial cuff, which also appeared in our simulations. However, exactly the same change in transit time was observed by altering brachial compliance only, indicating that PWV_{ATG} is only dependent on brachial stiffness and not on stiffness in the remaining part of the arterial tree. Wave intensity analysis also showed that the wave causing the second peak in the pressure signal is travelling back and forth between the occlusion and the location where the subclavian artery branches off from the aorta, and is not originating from a reflection in the lower body. Despite this, numerical values of PWV_{ATG} correlate well to standard methods such as the carotid-femoral transit time or the theoretical Bramwell-Hill equation, but the Arteriograph yields lower absolute values. A possible explanation for this correlation is that the stiffness of the upper brachial segment is likely to be related to aortic stiffness. Finally, one should keep in mind that this is a numerical study aiming to test the theoretical principle behind the Arteriograph, and we cannot make any judgement on the functioning of the device itself. An independent clinical study would be needed to confirm our results and to test the robustness of the device and its algorithms when confronted with non-theoretical measurement data.

Acknowledgements

Research funded by a Ph.D grant to the first author of the Institute for the Promotion of Innovation through Science and Technology in Flanders (IWT-Vlaanderen). The authors have no conflicts of interest to disclose.

References

[1] Baulmann, J., U. Schillings, S. Rickert, S. Uen, R. Dusing, M. Illyes, A. Cziraki, G. Nickering and T. Mengden. A new oscillometric method for assessment of arterial stiffness: comparison with tonometric and piezo-electronic methods. Journal of Hypertension. 26:523-528, 2008.
[2] Benyu, J., L. Baoming, K.L. McNeill and P.J. Chowienczyk. Measurement of pulse wave velocity using pulse wave Doppler ultrasound: comparison with arterial tonometry. Ultrasound in Medicine & Biology. 509-512, 2008.
[3] Bjarnegard, N. and T. Lanne. Arterial properties along the upper arm in man - age-related effects and the consequence of anatomical location. J Appl Physiol. epub ahead of print, 2009.
[4] Bonny, A., F. Lacombe, M. Yitemben, B. Discazeaux, J. Donetti, P. Fahri, R. Megbemado and B. Estampes. The 2007 ESH/ESC Guidelines for the management of arterial hypertension. Journal of Hypertension. 26:825-825, 2008.
[5] Bramwell, J.C. and A.V. Hill. The velocity of the pulse wave in man. Proc Soc Exp Biol Med. 93:298–306, 1922.
[6] Chiu, Y.C., P.W. Arand, S.G. Shroff, T. Feldman and J.D. Carroll. Determination of pulse wave velocities with computerized algorithms. Am Heart J. 121:1460-1470, 1991.
[7] Horvath, I., L. Papp and M. Illyes. Invasive Validations of a User Independent Oscillometric Device (Arteriograph) for Measuring Augmentation Index and Aortic Pulse Wave Velocity Artery Research 1:75-76, 2007.
[8] Illyes, M. A new and fast screening method for measuring complex hemodynamical parameters and arterial stiffness non-invasively with a simple arm cuff. American Journal of Hypertension. 18:15A-15A, 2005.
[9] Laurent, S., J. Cockcroft, L. Van Bortel, P. Boutouyrie, C. Giannattasio, D. Hayoz, B. Pannier, C. Vlachopoulos, I. Wilkinson, H. Struijker-Boudier and N.-i. European Network. Expert consensus document on arterial stiffness: methodological issues and clinical applications. European Heart Journal. 27:2588-2605, 2006.
[10] Lehmann, E.D. Noninvasive measurements of aortic stiffness: methodological considerations. Pathologie Biologie. 47:716-730, 1999.
[11] Magometschnigg, D. Blood pressure and arterial stiffness. A comparison of two devices for measuring augmentation index and pulse wave velocity. Wien Med Wochenschr. 155:404-410, 2005.
[12] Millasseau, S.C., A.D. Stewart, S.J. Patel, S.R. Redwood and P.J. Chowienczyk. Evaluation of carotid-femoral pulse wave velocity: influence of timing algorithm and heart rate. Hypertension. 45:222-226, 2005.
[13] Oliver, J.J. and D.J. Webb. Noninvasive assessment of arterial stiffness and risk of atherosclerotic events. Arteriosclerosis Thrombosis and Vascular Biology. 23:554-566, 2003.
[14] Parker, K.H. and C.J.H. Jones. Forward and backward running waves in the arteries - analysis using the method of characteristics. Journal of Biomechanical Engineering-Transactions of the Asme. 112:322-326, 1990.
[15] Reymond, P., F. Merenda, F. Perren, D. Rufenacht and N. Stergiopulos. Validation of a one-dimensional model of the systemic arterial tree. American Journal of Physiology-Heart and Circulatory Physiology. 297:H208-H222, 2009.
[16] Rietzschel, E.R., M.L. De Buyzere, S. Bekaert, P. Segers, D. De Bacquer, L. Cooman, P. Van Damme, P. Cassiman, M. Langlois, P. van Oostveldt, P. Verdonck, G. De Backer, T.C. Gillebert and I. Asklepios. Rationale, design, methods and baseline characteristics of the Asklepios Study. European Journal of Cardiovascular Prevention & Rehabilitation. 14:179-191, 2007.

[17] Segers, P., J. Kips, B. Trachet, A. Swillens, S. Vermeersch, D. Mahieu, E. Rietzschel, M. De Buyzere and L. Van Bortel. Limitations and pitfalls of non-invasive measurement of arterial pressure wave reflections and pulse wave velocity. Artery Research. 3:79-88, 2009.
[18] Segers, P., E. Rietzschel, S. Vermeersch, M. De Buyzere, D. De Bacquer, G. De Backer, P. Verdonck, T. Gillebert, L. Bortel and I. Asklepios. Carotid artery structure and large artery stiffness in 2524 middle-aged men and women (asklepios study): Integrating morphology and mechanics. Journal of Hypertension. 26:S63-S63, 2008.
[19] Stergiopulos, N., D.F. Young and T.R. Rogge. Computer simulation of arterial flow with applications to arterial and aortic stenoses. Journal of Biomechanics. 25:1477-1488, 1992.
[20] Swillens, A. and P. Segers. Assessment of arterial pressure wave reflection: Methodological considerations. Artery Research. 2:122-131, 2008.
[21] Van Bortel, L.M., E.J. Balkestein, J.J. van der Heijden-Spek, F.H. Vanmolkot, J.A. Staessen, J.A. Kragten, J.W. Vredeveld, M.E. Safar, H.A.S. Boudier and A.P. Hoeks. Non-invasive assessment of local arterial pulse pressure: comparison of applanation tonometry and echo-tracking. Journal of Hypertension. 19:1037-1044, 2001.
[22] Vermeersch, S.J., E.R. Rietzschel, M.L. De Buyzere, D. De Bacquer, G. De Backer, L.M. Van Bortel, T.C. Gillebert, P.R. Verdonck, P. Segers and I. Asklepios. Age and gender related patterns in carotid-femoral PWV and carotid and femoral stiffness in a large healthy, middle-aged population. Journal of Hypertension. 26:1411-1419, 2008.
[23] Westerhof, N., P. Sipkema, Vandenbo.Gc and G. Elzinga. Forward and backward waves in arterial system. Cardiovascular Research. 6:648-656, 1972.

Figure Legends

Figure 1. Illustration of the working principle of the Arteriograph. We refer to the text for details.

Figure 2. Representation of the arterial topology used in the computer model (adapted from [15]). In the occluded model, segments 22-25 were removed in order to simulate the occlusion of the brachial artery by the cuff.

Figure 3. Pressure waveforms at location of the cuff (brachial artery) for 3 levels of total arterial compliance (in % of the default value). Top left: Normal model. Top right: Occluded model, compliance altered in all segments. Bottom left: Occluded model, compliance altered only in brachial segments. Bottom right: Occluded model, compliance altered in all segments except the brachial segments.

Figure 4. Correlation between different methods to compute pulse wave velocities with varying model parameters Resistance (R), Heart cycle length (HC) and maximal heart Elastance (Emax). Top: Carotid-femoral PWV vs Theoretical PWV. Middle: Arteriograph PWV vs Theoretical PWV. Bottom: Arteriograph PWV vs Carotid-femoral PWV.

Figure 5. Correlation between different methods to compute pulse wave velocities when altering compliance only at the brachial segments, when altering compliance in all segments except the brachial segments, and when altering compliance in all segments

(default). Left: Arteriograph PWV vs Theoretical PWV. Right: Arteriograph PWV vs. carotid-femoral PWV.

Figure 6. Pressure waveforms at 6 locations throughout the brachial artery (distances are expressed in cm distal from aortic root). Top: Total pressure; Middle: Forward pressure; Bottom: Backward pressure.

Figure 7. Pressure waveforms at 6 locations throughout the descending and abdominal aorta (distances are expressed in cm distal from aortic root). Top: Total pressure; Middle: Forward pressure; Bottom: Backward pressure.

Figure 8. Wave intensity analysis at the location of the cuff (brachial artery) for C=100%. Bottom: Wave intensity analysis in normal model (left) and occluded model (right). Top: Effect of wave intensity on pressure signal and forward and backward pressure components in normal model (left) and occluded model (right).

Figures

Figure 1

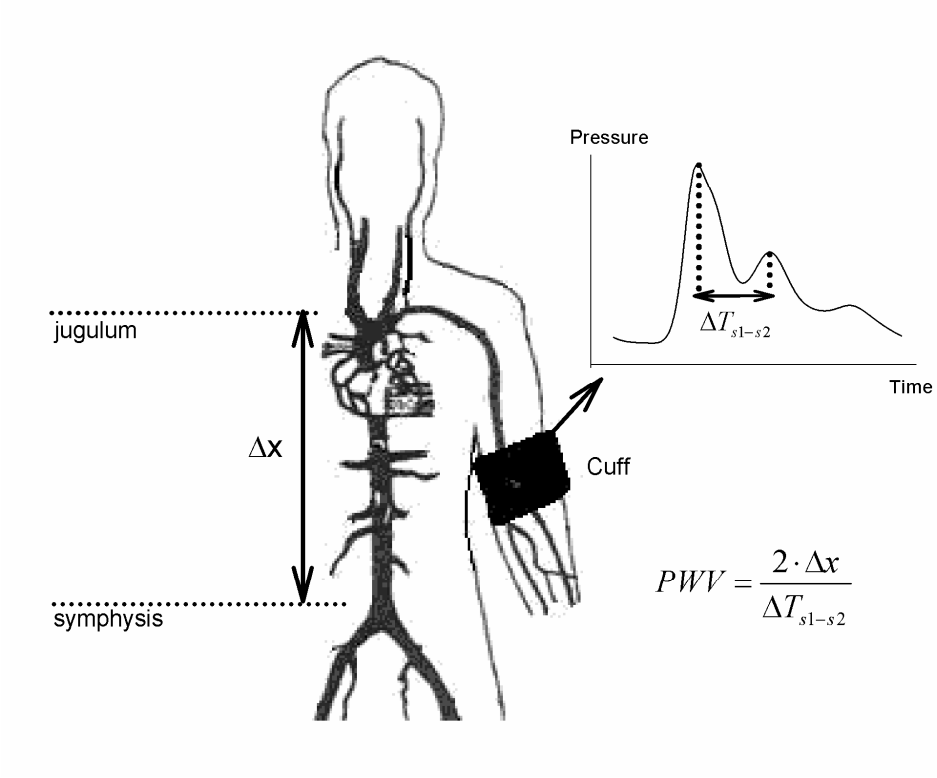

Figure 2

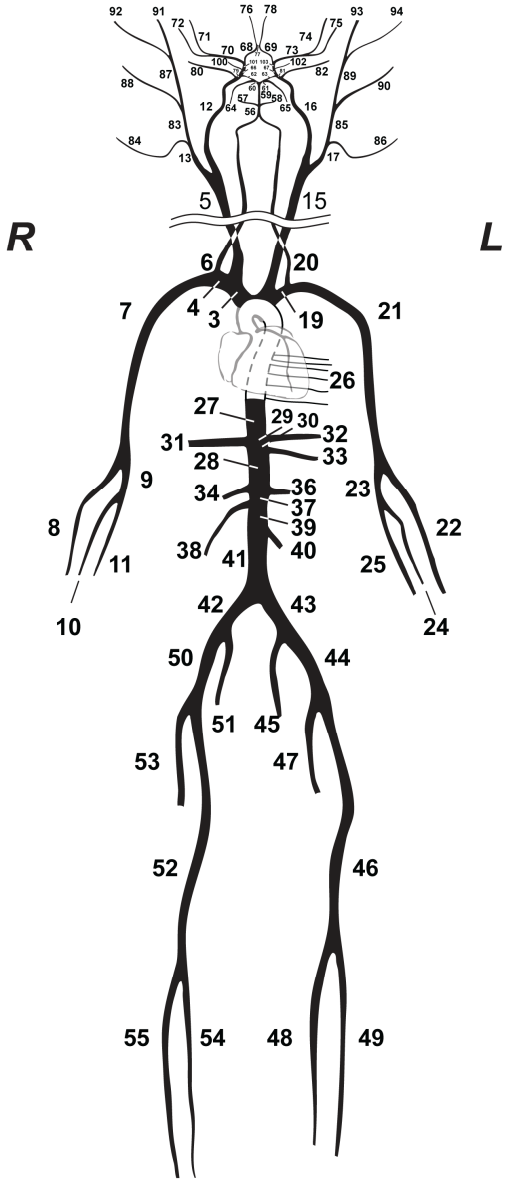

adapted from Reymond et al.

Figure 3

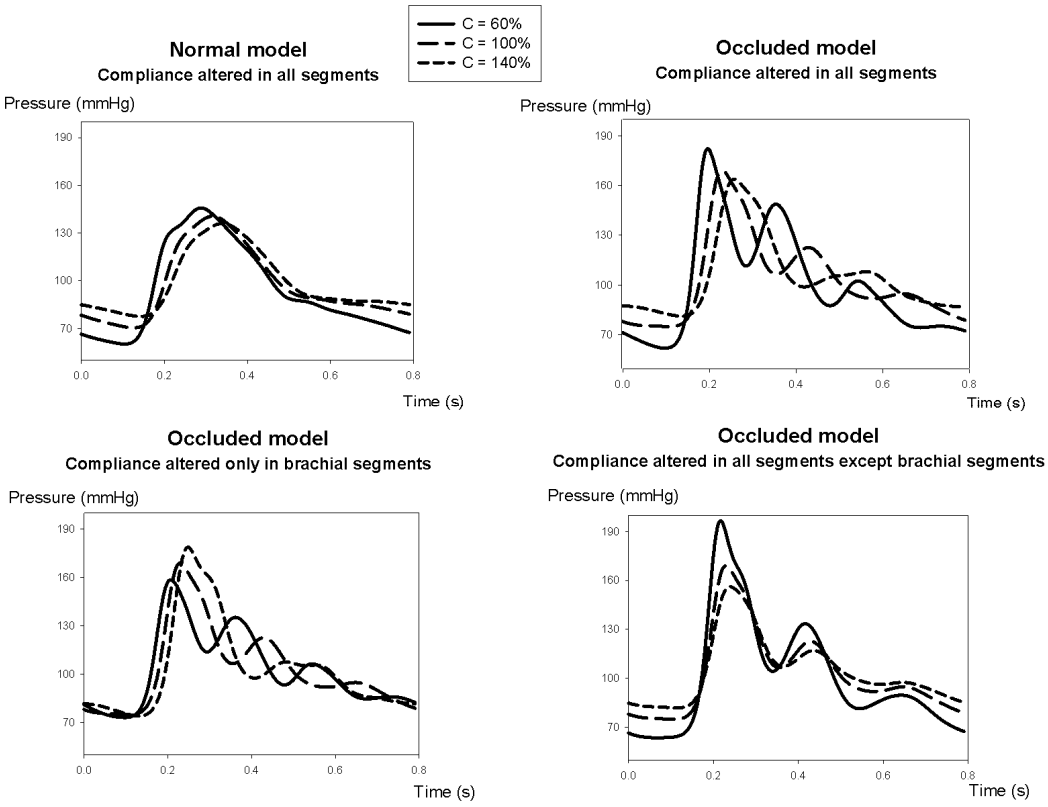
C = 60%
C = 100%
C = 140%
Normal model
Compliance altered in all segments
Pressure (mmHg)
190
160
130
100
70
0.0
0.2
0.4
0.6
0.8
Time (s)
Occluded model
Compliance altered in all segments
Pressure (mmHg)
Time (s)
Occluded model
Compliance altered only in brachial segments
Pressure (mmHg)
Time (s)
Occluded model
Compliance altered in all segments except brachial segments
Pressure (mmHg)
Time (s)

Figure 4

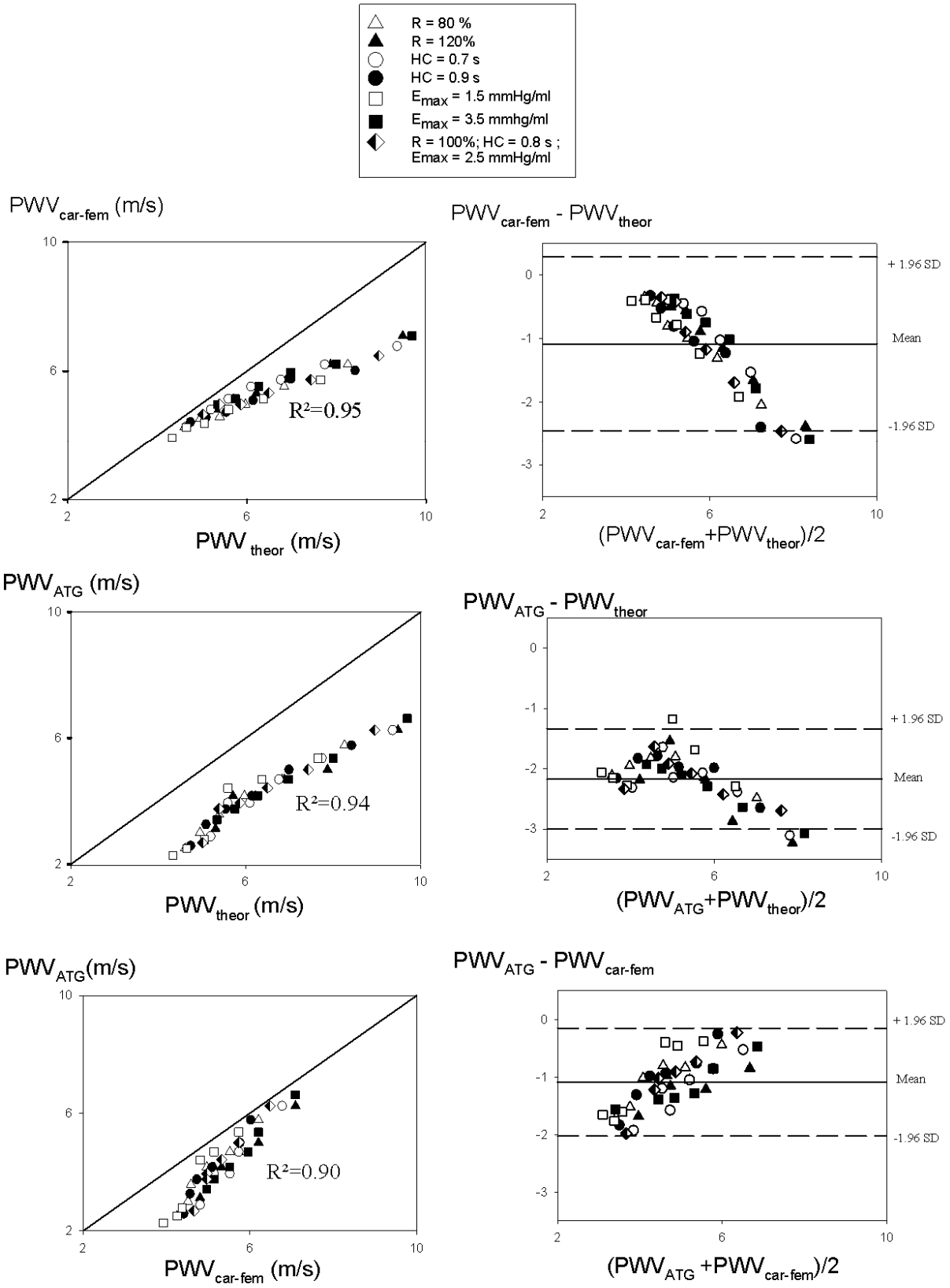
R = 80 %
R = 120%
HC = 0.7 s
HC = 0.9 s
Emax = 1.5 mmHg/ml
Emax = 3.5 mmhg/ml
R = 100%; HC = 0.8 s ; Emax = 2.5 mmHg/ml
PWVcar-fem (m/s)
PWVtheor (m/s)
R²=0.95
PWVcar-fem - PWVtheor
(PWVcar-fem+PWVtheor)/2
+ 1.96 SD
Mean
-1.96 SD
PWVATG (m/s)
PWVtheor (m/s)
R²=0.94
PWVATG - PWVtheor
(PWVATG+PWVtheor)/2
PWVATG(m/s)
PWVcar-fem (m/s)
R²=0.90
PWVATG - PWVcar-fem
(PWVATG +PWVcar-fem)/2

Figure 5

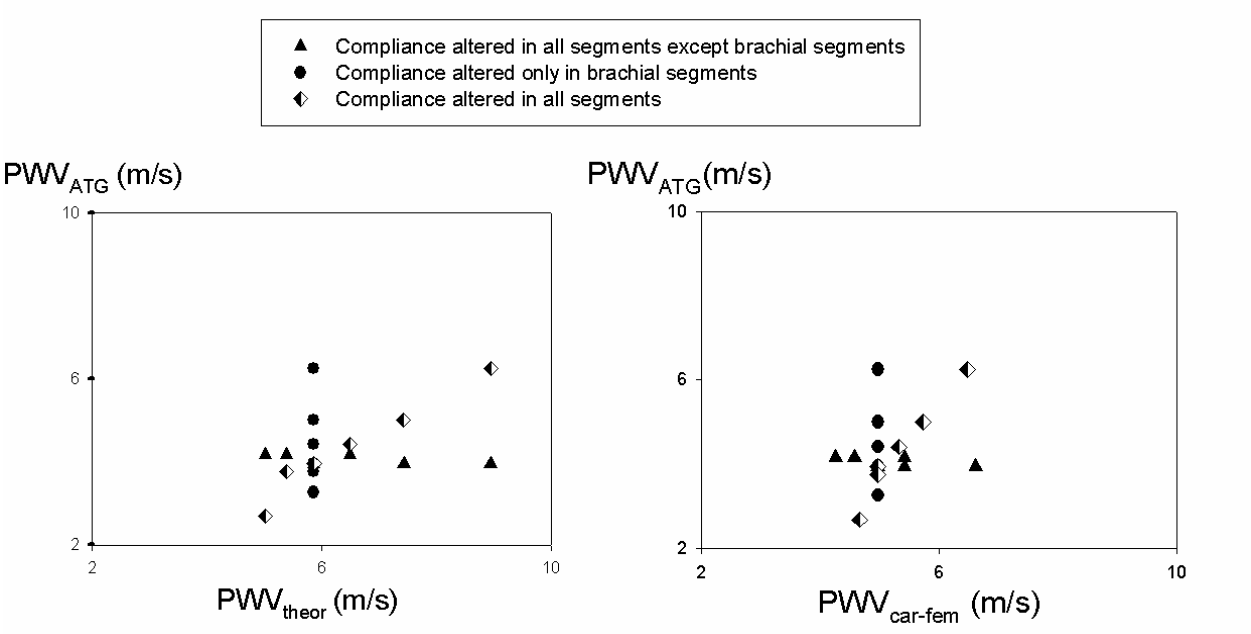
Compliance altered in all segments except brachial segments
Compliance altered only in brachial segments
Compliance altered in all segments
PWV_ATG (m/s)
10
6
2
2
6
10
PWV_theor (m/s)
PWV_ATG(m/s)
10
6
2
2
6
10
PWV_car-fem (m/s)

Figure 6

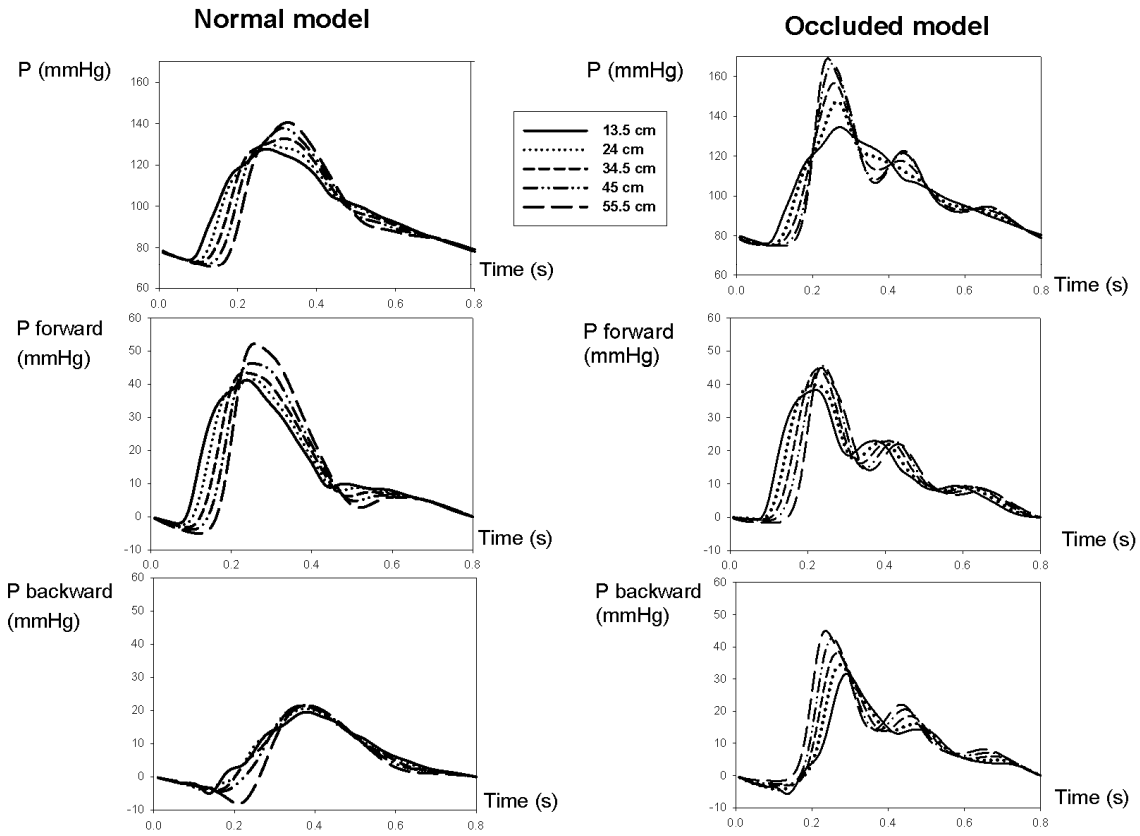
Normal model
Occluded model
P (mmHg)
P forward (mmHg)
P backward (mmHg)
Time (s)
13.5 cm
24 cm
34.5 cm
45 cm
55.5 cm

Figure 7

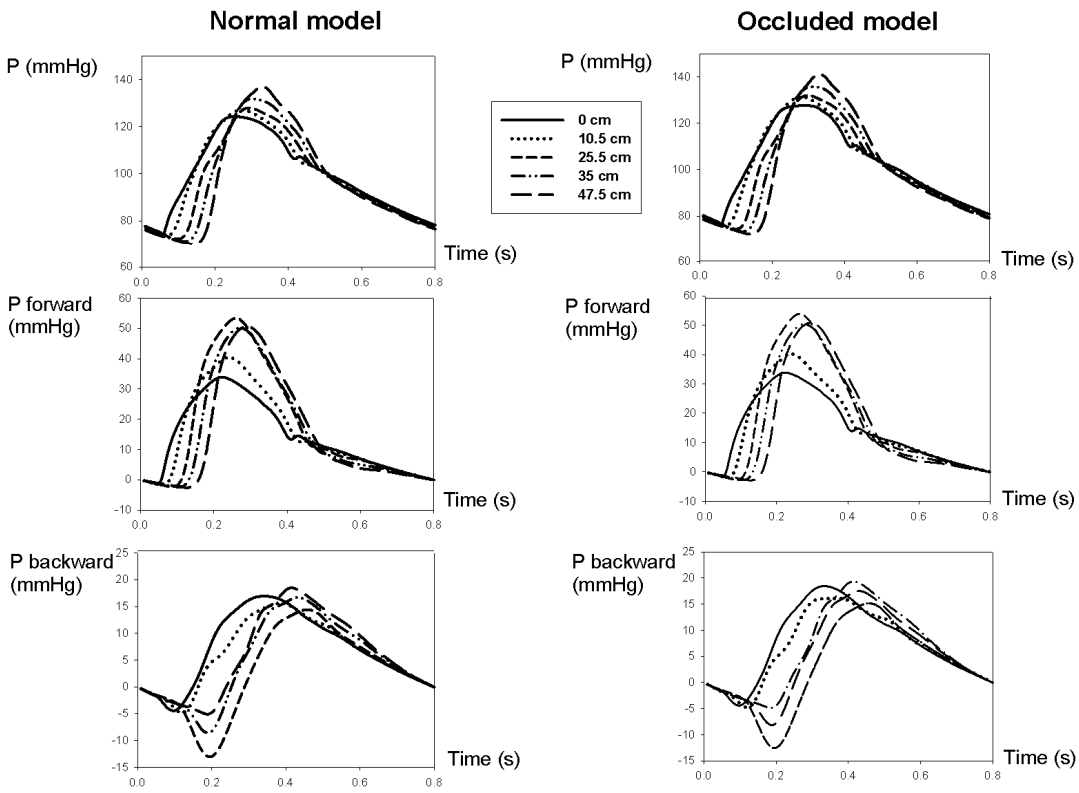
Normal model
Occluded model
P (mmHg)
P forward (mmHg)
P backward (mmHg)
Time (s)
0 cm
10.5 cm
25.5 cm
35 cm
47.5 cm

Figure 8

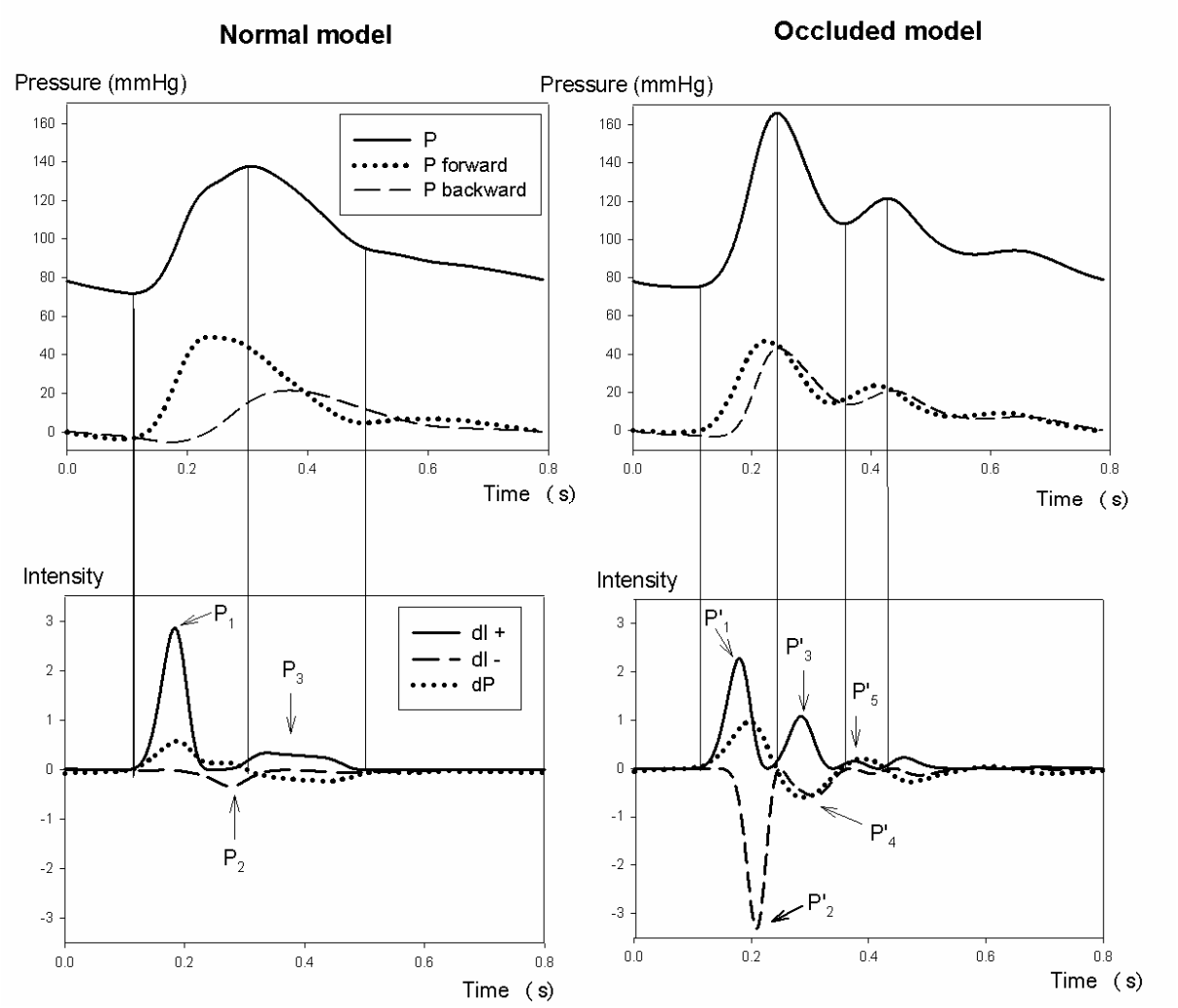
Normal model
Occluded model
Pressure (mmHg)
Pressure (mmHg)
P
P forward
P backward
Time (s)
Time (s)
Intensity
Intensity
dI +
dI -
dP
P1
P2
P3
P'1
P'2
P'3
P'4
P'5
Time (s)
Time (s)